Separation of a diastereomeric diol pair using mechanical properties of crystals

Gamidi Rama Krishna,[a]* Monica Dandawate,[a] Srinu Tothadi,[a] Rahul Choudhury,[a,b] Ashwini K. Nangia,[a,c]* and D. Srinivasa Reddy,[a,b]*

[a] *Organic Chemistry Division, CSIR-National Chemical Laboratory, Dr. Homi Bhabha Road, Pune 411008, India*

[b] *Academy of Scientific and Innovative Research (AcSIR), Ghaziabad 201002, India.*

[c] *School of Chemistry, University of Hyderabad, Hyderabad 500046, India*

Corresponding authors: e-mail: rk.gamidi@ncl.res.in (GRK) ds.reddy@ncl.res.in (DSR) and ashwini.nangia@gmail.com (AKN)

Experimental Procedure

Derivatization Reactions

The synthesis of diastereomers and analytical characterization are extracted from our recent paper[S1] (ref. 35 of the paper) and reproduced. All the derivatization reactions were carried out in oven-dried glassware under a positive pressure of argon or nitrogen, unless otherwise mentioned, with magnetic stirring. Air-sensitive reagents and solutions were transferred *via* a syringe or cannula and were introduced into the apparatus *via* rubber septa. All reagents, starting materials, and solvents were obtained from commercial suppliers and used without further purification. Reactions were monitored by thin-layer chromatography (TLC), as mentioned below. Column chromatography was performed on silica gel (100−200 or 230−400 mesh size). Deuterated solvents for NMR spectroscopic analyses were used as received. All ^{1}H-NMR and ^{13}C-NMR spectra were obtained using 200, 400, or 500 MHz spectrometers. Coupling constants were measured in Hertz. All chemical shifts were quoted in ppm, relative to $CDCl_3$ and Methanol- d_4 (CD_3OD), using the residual solvent peak as a reference standard. The following abbreviations were used to explain the multiplicities: s = singlet, d = doublet, t = triplet, q = quartet, dd = doublet of doublet, dq = doublet of quartet, m = multiplet, br = broad. HRMS (ESI) was recorded on an ORBITRAP mass analyzer (Thermo Scientific, Q Exactive). Mass spectra were recorded with ESI ionization in an MSQ LCMS mass spectrometer. Infrared (IR) spectra were recorded on a Fourier transform infrared spectrometer as a thin film. Chemical nomenclature was generated using Chem Bio Draw Ultra 14.0.

(5S)-4-allyl-5-benzyl-4-ethyl-2,2-dimethyl-1,3-dioxolane (1a)

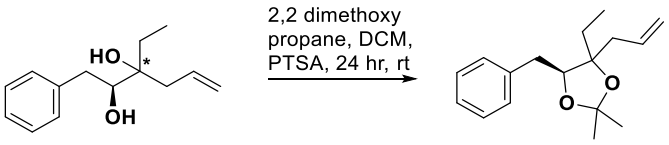

1a

A mixture of **(2*S*)-3-ethyl-1-phenylhex-5-ene-2, 3-diol (ephd)** (0.30 g, 1.36 mmol, 1 equiv.), *p*-TsOH.H_2O (0.06 g, 0.0816 mmol, 0.06 equiv.), and 2, 2'-dimethoxy propane (0.84 mL, 0.85 g, 8.17 mmol, 6 equiv.) in 15 mL of dichloromethane was stirred at rt for 24 h. The reaction mixture was quenched with 10 mL of a saturated sodium bicarbonate solution. The aqueous layer was extracted with ethyl acetate (3x20 mL). Organic layers were combined, dried over anhydrous sodium sulfate, and filtered. The filtrate was concentrated under the *vacuum*. The crude product was purified using silica gel column chromatography to afford **1a** (0.292 g, 82%) as a sticky pale yellow liquid.

IRυ_{max} (film) : 2924.21, 2859.61, 1692.94, 1452.69, 1371.94, 1251.09, 1184.18, 1084.49, 1037, 916.66, 737.82 cm^{-1}. **^{1}H NMR (400 MHz, $CDCl_3$)** (Diastereomeric mixture) **δ** 7.31 – 7.17 (m, 5H), 5.97 – 5.72 (m, 1H), 5.01 (dddd, *J* = 17.1, 6.5, 4.7, 1.2 Hz, 2H), 4.14 (dt, *J* = 8.7, 4.5 Hz, 1H), 2.89

(ddd, *J* = 25.3, 14.4, 8.9 Hz, 1H), 2.71 (dd, *J* = 14.3, 4.2 Hz, 1H), 2.54 – 2.37 (m, 1H), 2.16 – 2.00 (m, 1H), 1.77 – 1.62 (m, 1H), 1.44 (d, *J* = 16.5 Hz, 3H), 1.37 (ddd, *J* = 14.6, 10.9, 7.0 Hz, 1H), 1.29 (d, *J* = 6.0 Hz, 3H), 0.92 (dt, *J* = 45.5, 7.5 Hz, 3H). **^{13}C NMR (100 MHz, $CDCl_3$)** (Diastereomeric mixture) **δ** 138.87, 134.35, 133.87, 129.19, 129.05, 128.57, 128.51, 126.51, 126.44, 118.27, 118.14, 107.09, 106.85, 83.68, 83.35, 81.69, 80.96, 39.30, 38.78, 35.76, 35.42, 28.68, 28.60, 27.82, 26.99, 26.91, 26.31, 8.13, 7.42. **HRMS (ESI):** *m*/*z* calculated for $C_{17}H_{24}O_2Na$ $[M+Na]^+$ 283.1674, found 283.1669.

(2*S*)-3-ethyl-1-phenylhex-5-ene-2, 3-diol (ephd) (0.30 g, 1.36 mmol, 1 equiv) was dissolved in MTBE (methyl tertiary butyl ether). Vinyl acetate (0.35 g, 4.08 mmol, 3 equiv), Na_2CO_3 (0.119 g, 1.129 mmol, 0.83 equiv), and Lipase (Amano P. S.) (80 mg) was added. The reaction mixture was stirred at 30 °C for 24 h and monitored reaction by TLC. There is no kinetic resolution observed. The organic layer was filtrated and recovered the starting material.

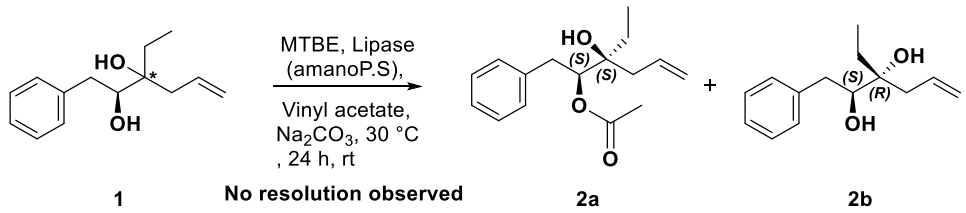

The round bottom flask was loaded with (*S*)-2-hydroxy-1-phenylpentan-3-one (0.5 g, 2.8 mmol, 1 equiv) and Indium powder (0. 322 g, 2.8 mmol, 1 equiv) in THF/H_2O (2:1). The solution was stirred for 5 to 10 mins followed by careful addition of allyl bromide (0.5 g, 4.2 mmol, 1.5 equiv, 1.4 mL) was carried out, and the reaction mixture was allowed to stir for 6 h at 32 °C. The progression of the reaction was monitored using TLC. The reaction was carefully quenched using saturated NH_4Cl (25 mL) and extracted with EtOAc (3 x 20 mL). The organic layer was washed with brine (20 mL), dried over sodium sulfate, and concentrated under reduced pressure. The residue was purified by column chromatography to give diol **1** a white solid (520 mg 84%).

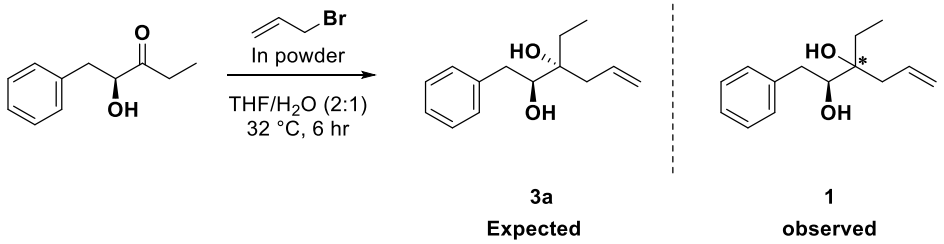

IRυ_{max}(film): 3562, 3413, 3334, 2852, 1513, 1210 cm^{-1}. **^{1}H NMR (400 MHz, $CDCl_3$)** (Diastereomeric mixture) **δ** 7.36 – 7.32 (m, 2H), 7.28 – 7.24 (m, 3H), 6.01 – 5.89 (m, 1H), 5.23 – 5.15 (m, 2H), 3.79 – 3.74 (m, 1H), 2.94 (dd, *J* = 13.7, 2.1 Hz, 1H), 2.64 (dt, *J* = 13.7, 9.9 Hz, 1H), 2.57 – 2.45 (m, 1H), 2.42 – 2.23 (m, 1H), 2.16 (d, *J* = 16.5 Hz, 1H), 1.91 – 1.66 (m, 2H), 1.54 (dq, *J* = 14.8, 7.5 Hz, 1H), 1.01 (t, *J* = 7.5 Hz, 3H); **^{13}C NMR (100 MHz, $CDCl_3$)** (Diastereomeric mixture) **δ** 139.2, 134.2, 133.9, 129.5, 129.5, 128.8, 126.7, 118.8, 118.4, 76.4, 75.7, 75.5, 40.3, 39.1, 37.7, 37.5, 28.9, 27.3, 7.7, 7.6; **HRMS (ESI):** *m*/*z* calculated for $C_{14}H_{20}O_2Na$ $[M+Na]^+$ 243.1361, found 243.1362.

(2S)-3-ethyl-3-hydroxy-1-phenylhex-5-en-2-yl 4-nitrobenzoate

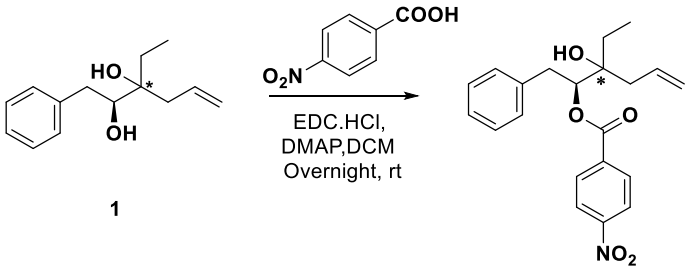

A mixture of **(2*S*)-3-ethyl-1-phenylhex-5-ene-2, 3-diol (ephd)** (0.18 g, 0.8 mmol, 1 equiv) was taken in dry dichloromethane at 0 °C under stirring condition. EDC.HCl (0.23 g, 1.24 mmol, 1.5 equiv) and DMAP (101 mg, 0.828 mmol) were added. The mixture was allowed to stir for 5 min and *p*-nitro benzoic acid was added to the reaction mixture. The reaction was stirred for 2 h at 0 °C and left at room temperature overnight. The reaction mixture was quenched with water (10 mL) and washed with 2N HCl (20 mL) followed by $NaHCO_3$ (20 mL) and brine (20 mL). The organic layer was dried over sodium sulfate and concentrated in *vacuo*. The crude was purified by column chromatography to get 0.212 g (70% yield) as a white solid. IR υmax: 3860.42 3590.38, 3477.38, 2960.67, 1723.65, 1527.76, 1344.58, 1273.14, 1110.57, 1005.55, 713.98 cm^{-1}. **^{1}H NMR (400 MHz, $CDCl_3$)** (Diastereomeric mixture) δ 8.25 – 8.22 (m, 2H), 8.07 – 8.04 (m, 2H), 7.17 (d, J = 4.3 Hz, 4H), 7.14 – 7.09 (m, 1H), 5.98 – 5.88 (m, 1H), 5.47 (td, J = 11.0, 3.1 Hz, 1H), 5.24 – 5.15 (m, 2H), 3.17 (ddd, J = 14.1, 9.4, 3.0 Hz, 1H), 3.04 – 2.97 (m, 1H), 2.49 – 2.33 (m, 2H), 1.89 (bs, 1H), 1.82 – 1.63 (m, 2H), 1.03 (t, J = 7.5 Hz, 3H). **^{13}C NMR (100 MHz, $CDCl_3$)** (Diastereomeric mixture) δ 164.20, 150.63, 137.53, 135.51, 132.84, 132.75, 130.73, 129.51, 129.36, 128.57, 128.42, 126.78, 123.65, 119.63, 80.15, 75.80, 75.55, 40.83, 39.72, 35.75, 29.21, 28.46, 7.71. **HRMS (ESI): m/z** calculated for $C_{21}H_{24}O_5N$ $[M+H]^+$ 370.1649, found 370.1652.

Preparation of single crystals of ephd diastereomers

The mixture of **ephd** compound dissolved in the dichloromethane/n-hexane solvent and heated to get the clear solution. The solution was filtered through the Whatman filter paper in a dry and clean conical flask and kept for slow evaporation at room temperature. Notably, the single crystals of both the diastereomers ((2*S*,3*S*)-**ephd** and (2*S*,3*R*)-**ephd**) were harvested after 2-3 days with acicular morphology. About the length of the crystal's up to 0.5 cm (see Figure 2 of the paper). The single crystals were suitable for SCXRD measurements and to perform mechanical experiments. Notably, the crystallization experiments were carried out in various organic solvents; however, the best quality crystals were obtained using a combination of dichloromethane/n-hexane solvent.

Separation of ephd diastereomers by mechanical methods

As a primary step, the polarity and separation of diastereomers were monitored by thin-layer chromatography (TLC) with 0.25 mm precoated silica gel plates (60 F254). Various combinations of mobile phases were used to separate both the diastereomers. Unfortunately, none of them were successful, which was confirmed by visualizing the TLC spots under a UV lamp or various stain solutions. For instance, phosphomolybdic acid, *p*–anisaldehyde, vanillin, and $KMnO_4$ solution or iodine adsorbed on silica gel, followed by heating with hot air gun for ~15 s.

As a next step, mechanical methods were employed to separate the single crystals of **ephd** diastereomers. Herein, the experiments were carried out by applying the mechanical force using metal forceps and needles by viewing the molecular crystals under a polarized microscope. The

investigation was carried out by taking ~50 mg of the diastereomeric mixture, and we ended up with approximately 30 mg of (2*S*,3*S*)–**ephd** and 20 mg of (2*S*,3*R*)–**ephd** diastereomer. The overall process of separation has been completed over 30 min.

PXRD: The phase purity of the separated molecular crystals of diastereomers was examined by PXRD experiments. The experiments were carried out at RT on a APEX3 (Bruker, 2016; Bruker D8 VENTURE Kappa Duo PHOTON II CPAD) diffractometer having graphite–monochromatized (Cu = 1.54178 Å). The experiments were carried by the capillary method. The X-ray generator was operated at 50 kV and 30 mA. The obtained diffraction patterns compared with simulated PXRD patterns obtained from the SCXRD experiments (Figure S3), which was reported in our earlier studies.[1]

Melting point: The melting point of diastereomers was measured in a Buchi B–540 melting point apparatus; the obtain melting point value for (2*S*,3*S*)–**ephd** is 90.5 °C, while the melting point of (2*S*,3*R*)–**ephd** is 91.5 °C.

SCXRD Experiments: SCXRD experiments were performed for both the diastereomers at 100 K using APEX3 (Bruker, 2016; Bruker D8 VENTURE Kappa Duo PHOTON II CPAD) diffractometer having graphite–monochromatized (Cu = 1.54178 Å). The X-ray generator was operated at 50 kV and 30 mA. A preliminary set of unit cell parameters and an orientation matrix were calculated from a total of 40 frames, and the cell refinement was performed by SAINT–Plus (Bruker, 2016). An optimized strategy used for data collection consisted of different sets of φ and ω scans with 0.5° steps φ/ω. The data were collected with a time frame of 10 sec by setting the sample to detector distance fixed at 40 cm. The data points were corrected for Lorentzian, polarization, and absorption effects using SAINT–Plus and SADABS programs (Bruker, 2016). SHELXS–97 (Sheldrick, 2008)[S2] was used for structure solution and full-matrix least-squares refinement on F^2. The molecular graphics of ORTEP diagrams of both the diastereomers were performed by X-Seed software package version 2.0.[S3] The crystal symmetry of both the diastereomers is cross-checked by running the cif files PLATON (Spek, 2020) software and notified that no additional symmetry was observed. The Encifer software was used to correct the cif files.

We previously reported[S1] (ref. 35 of paper) the absolute configuration of each diastereomer through SCXRD experiments performed at RT using Cu-Kα as the X-ray source. Notably, there was an issue of the double bond distance of a propylene group in the (2*S*,3*R*)-**ephd** diastereomer. Such that it gave a very short bond distance (1.03 Å) compared to the usual bond length (1.34 Å, e,g. in the (2*S*,3*S*)-**ephd** diastereomer the double bond length is 1.29 Å). Because the experiment was performed at RT, due to high atomic vibrations around the double bond, there is the elongation of thermal ellipsoids for these allyl group carbon atoms (visible in the visualization of cif structure). To resolve this issue, the SCXRD experiment of (2*S*,3*R*)-**ephd** was redetermined at 100 K. The LT (100 K) and RT (298 K) crystallographic data sets are listed in Table S1. Upon noticing that the unit cell of (2*S*,3*R*)-**ephd** in $P2_1$ space group doubles with a change in the Z' in measurements from RT to LT, we carried out a temperature variation study to study the temperature at which the transition in cell parameters occurs, which is observed at about 215-220 K (Table S2). The crystal system (monoclinic) and space group $P2_1$ remain the same, but the unit cell parameters differ from the unit cells in the RT to LT range. For instance, the cell volume doubled from 658.25(5)→ 1253.24(10) $Å^3$, the cell axis shifts from a = 10.4503(5) → 12.4200(6) Å; b = 5.1516(2) → 5.0966(2) Å, and c =12.7890(6) → 20.6491(9) Å, and the cell angle shifts from β = 107.0500(10) → 106.502(2) °. With the doubling of the unit cell at 100 K, the asymmetric unit contains two molecules (Z' = 2) (Table S1). The crystal packing arrangement in the LT structure is nearly similar to that in the RT structure (Figure S1), and the same is reflected in

the PXRD pattern (Figure S2). Based on these similarities, we assign the change in crystal structure parameters more as a modulation[S4] rather than a polymorph. The (2*S*,3*S*)-**ephd** diastereomer in space group $P2_12_12_1$ has identical crystal structures at LT and RT (Table S1 and S2, Figure S2), except for minor T variations. Subsequent discussion and analysis in this paper on (2*S*,3*R*)-**ephd** and (2*S*,3*S*)-**ephd** diastereomers is carried out using the LT data at 100 K (hydrogen bond Table S3 and Figure S3 to Figure S7).

Hirshfeld analysis

The Hirshfeld surfaces[S5] of each diastereomer were mapped with such that each point on the surface, the distances to the nearest atoms outside (intermolecular) *d*e, and inside (intramolecular) *d*i, are approximated and used for a color-coded map of the surfaces (Figure S8a and b). The deep red spots indicate closest contacts with neighboring molecules; the deep blue color means very little or no interaction with the surrounding molecules. While the 2D fingerprint plots of both the diastereomers were generated from the Hirshfeld surfaces, showing the arrangement of the *d*e distances as a function of *d*i. Each point in the fingerprint graph is colored according to the fraction of the total surface area, ranging from blue (few points) through green (moderate number of points) to red (many points) (Figure S8c and d). The decomposition of fingerprints with an appropriate percentage of characteristic intermolecular interactions is given in Figure S9. The O···H, C···H and H···H types of intermolecular interactions are observed in both cases. The most directional O···H type intermolecular interactions are higher in (2*S*,3*R*)-**ephd** than (2*S*,3*S*)-**ephd** (8.3% and 7.8%). The C···H type interaction percentages are slightly higher in (2*S*,3*S*)-**ephd** (15.3%) than (2*S*,3*R*)-**ephd** (14.4%), while the H···H type intermolecular interactions are similar percentages (76.5%, 76.6%). The interaction percentages show that the O···H interaction percentage is slightly higher in (2*S*,3*R*)-**ephd** and they run in orthogonal directions to the weak van der Waals interactions. The weak and strong interactions are well separated in the crystal packing arrangement, making the crystal structure anisotropic, which is uncommon (but not unprecedented) for elastic deformation in crystals. In (2*S*,3*S*)-**ephd,** the O···H interaction percentage is lower, while the C···H interactions are higher (the difference is albeit less than 1%). More significantly, the strong and weak interactions are not well separated in different domains/ directions of the structure and adopt an interlocked crystal packing arrangement. Hence the crystal structure arrangement becomes more isotropic. As a result, the molecular crystals undergo brittle deformation. The significant observation from these results is that even though the difference in the percentage of O···H and C···H type interactions is very slight, their impact on the mechanical properties of molecular crystals is enormous. We believe this is due to the anisotropic *vs*. interlocked packing arrangements between the elastic and brittle crystals. Thus the problem stated in Scheme S1 is solved by the methodology presented in the main paper.

Table S1. Crystallographic information of (2*S*,3*S*)–**ephd** and (2*S*,3*R*)–**ephd** at LT (100 K) in this study. Crystal data of the same compounds determined at RT in our previous study (TL paper, ref. 35) is reproduced for comparison.

Crystal data	Compound (2*S*,3*R*)–**ephd**	Compound (2*S*,3*S*)–**ephd**	Compound 4a (2*S*,3*R*)–**ephd**	Compound 4b (2*S*,3*S*)–**ephd**
	LT data (the present study)		RT data from the TL paper (ref. 35)	
Chemical formula	$C_{14}H_{20}O_2$	$C_{14}H_{20}O_2$	$C_{14}H_{20}O_2$	$C_{14}H_{20}O_2$
Formula weight (M_r)	220.30	220.30	220.30	
Crystal system	Monoclinic	Orthorhombic	Monoclinic	Orthorhombic
Space group	$P2_1$	$P2_12_12_1$	$P2_1$	$P2_12_12_1$

Temperature T (K)	100 (2)	100 (2)	298(2)	298(2)
a (Å)	12.4314 (16)	5.0851(17)	10.4503(5)	5.1521(10)
b (Å)	5.0981 (7)	13.6181(18)	5.1516(2)	13.809(3)
c (Å)	20.634 (3)	18.784(2)	12.7890(6)	18.891(4)
α (°)	90	90	90	90
β (°)	106.370 (4)	90	107.0500(10)	90
γ (°)	90	90	90	90
Z	4	4	2	4
Volume ($Å^3$)	1253.24(10)	1300.8(5)	658.25(5)	1344.0(5)
Source of radiation	Cu-Kα	Cu-Kα	Cu-Kα	Cu-Kα
D_{calc} (g cm^{-3})	1.166	1.125	1.111	1.089
Crystal size (mm)	0.48x 0.08x 0.07	0.44x0.11x0.096	0.52x0.04x0.03	0.54x0.1x0.09
Crystal description, color	Needle, colorless	Needle, colorless	Needle, colorless	Needle, colorless
μ (mm^{-1})	0.600	0.578	0.571	0.56
Flack parameter	0.04 (5)	0.04(7)	0.11(6)	0.05 (7)
Data collection				
Diffractometer	Bruker D8 VENTURE Kappa Duo PHOTON II CPAD	Bruker D8 VENTURE Kappa Duo PHOTON II CPAD	Bruker D8 VENTURE Kappa Duo PHOTON II CPAD	Bruker D8 VENTURE Kappa Duo PHOTON II CPAD
Absorption correction	Multi-scan (SADABS; Bruker, 2016)	Multi-scan (SADABS; Bruker, 2016)	Multi-scan (SADABS; Bruker, 2016)	Multi-scan (SADABS; Bruker, 2016)
T_{min}, T_{max}	0.512, 0.754	0.630, 0.754	0.545, 0.753	0.691, 0.754
No. of measured, independent and observed [I > 2σ(I)] reflections	26579, 4986, 4938	53763, 2552, 2446	17660, 2370, 2302	25430, 2629, 2371
Theta range (°)	3.8–74.8	5.73 – 72.64	8.6–70	5.7–71.9
R_{int}	0.055	0.069	0.047	0.043
h, k, l	$h = -15 \rightarrow 15$ $k = -6 \rightarrow 6$ $l = -25 \rightarrow 25$	$h = -6 \rightarrow 6$ $k = -16 \rightarrow 16$ $l = -23 \rightarrow 23$	$h = -12 \rightarrow 12$ $k = -6 \rightarrow 5$ $l = -15 \rightarrow 15$	$h = -5 \rightarrow 6$ $k = -17 \rightarrow 17$ $l = -23 \rightarrow 23$
Refinement				
$R[F^2 > 2\sigma(F^2)]$, $wR(F^2)$	0.0342	0.0338	0.056	0.036
GOF on F^2	1.03	1.069	1.10	1.05
No. of independent reflections	4986	2552	2370	2629
No. of parameters	295	149	155	154
No. of restraints	0	0	1	0
H-atom treatment	Constr	Constr	Constr	Constr
$\Delta\rho_{max}$, $\Delta\rho_{min}$ (e $A^{\circ -}$	0.22, −0.20	0.185, -0.159	0.26, −0.23	0.10, −0.08

^{3})				
CCDC number	2048024	2048025	2013534	2013535

Table S2. Transformation of unit cell parameters of (2*S*,3*R*)–**ephd** diastereomer as a function of temperature from 100 to 298 K. Crystal cell transformation (modulation) occurs at 215-220 K (shaded columns). The RT unit cell matches that determined in a previous study (ref. 35).

Diastereomer	Crystal system	Cell parameters	Temperature and unit cell parameters variation									
(2*S*,3*R*)–**ephd**	Monoclinic $P2_1$	T (K)	100	120	140	160	180	200	210	215	220	298
		a/Å	12.46	12.49	12.51	12.52	12.56	12.60	12.61	12.62	10.42	10.45
		b/Å	5.07	5.08	5.09	5.09	5.11	5.12	5.12	5.12	5.13	5.15
		c/Å	20.69	20.72	20.72	20.74	20.77	20.81	20.82	20.84	12.62	12.78
		α/°	90	90	90	90	90	90	90	90	90	90
		β/°	106.47	106.55	106.59	106.73	106.79	106.85	106.93	106.93	106.94	107.05
		γ/°	90	90	90	90	90	90	90	90	90	90
		V/Å^3	1253	1261	1265	1266	1275	1286	1286	1289	645	658

Table S3. Hydrogen-bond geometry (A˚, °) of compound (2*S*,3*R*)–**ephd** and compound (2*S*,3*S*)–**ephd** (100 K data).

Name of the compound	*D*–H···*A*	*D*–H	H···*A*	*D*···*A*	*D*–H···*A*
Compound (2*S*,3*R*)–**ephd**	O1−H1···O2	0.84	2.01	2.7659(19)	150
	O2−H2A···O1	0.84	1.88	2.714(2)	176
	O3–H3···O4	0.84	1.95	2.735(2)	156
	O4–H4···O3	0.84	1.84	2.683(2)	175
Compound (2*S*,3*S*)–**ephd**	O1−H1···O2	0.84	2.00	2.7586(18)	151
	O2−H2···O1	0.84	1.86	2.6950(17)	176

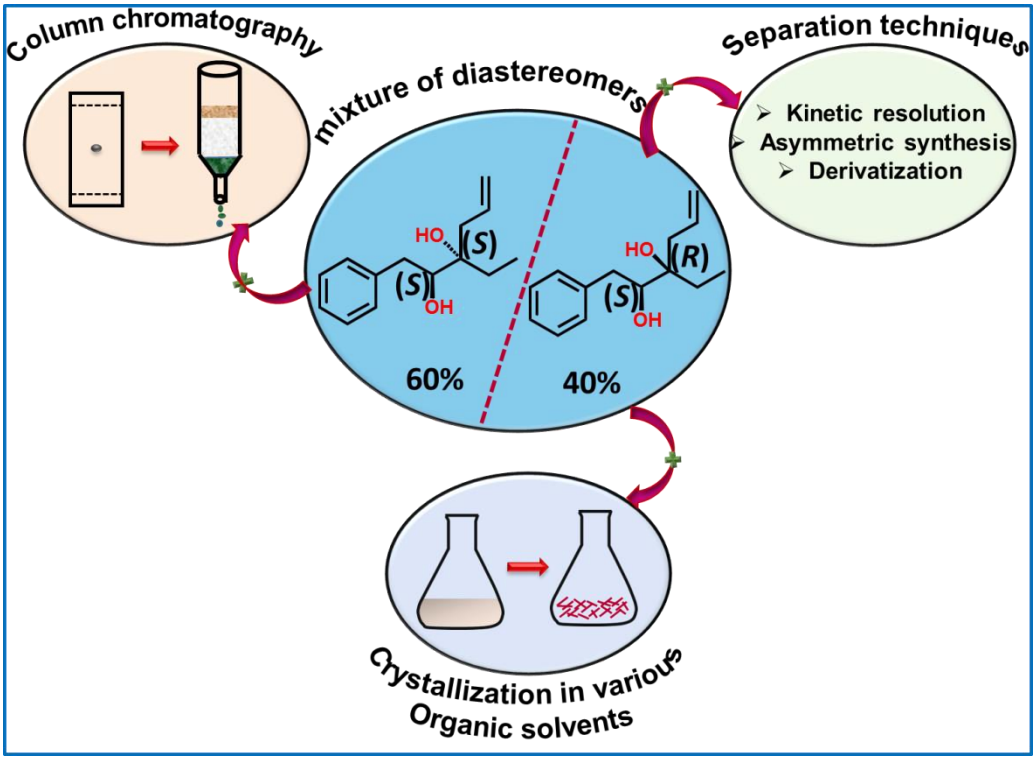

Scheme S1. The methods employed to separate the (2*S*)-3-ethyl-1-phenylhex-5-ene-2, 3-diol (**ephd**) diastereomers; however, none of the experiments were successful.

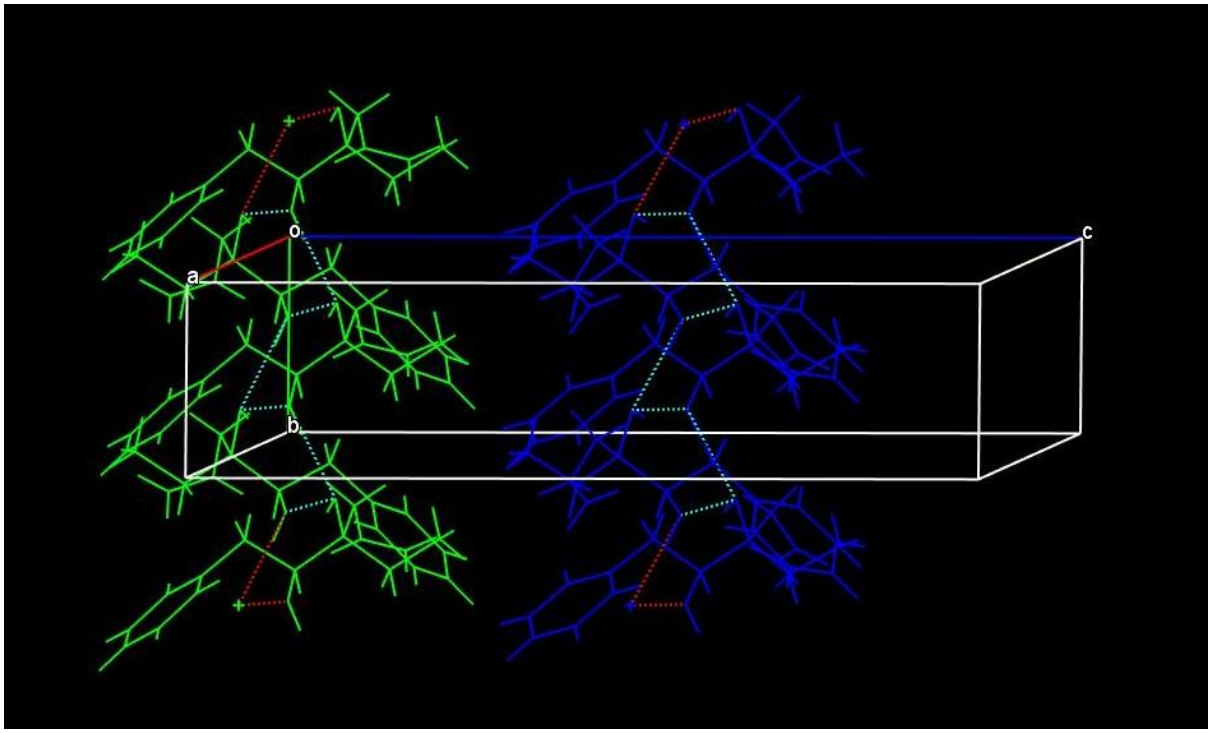

(a)

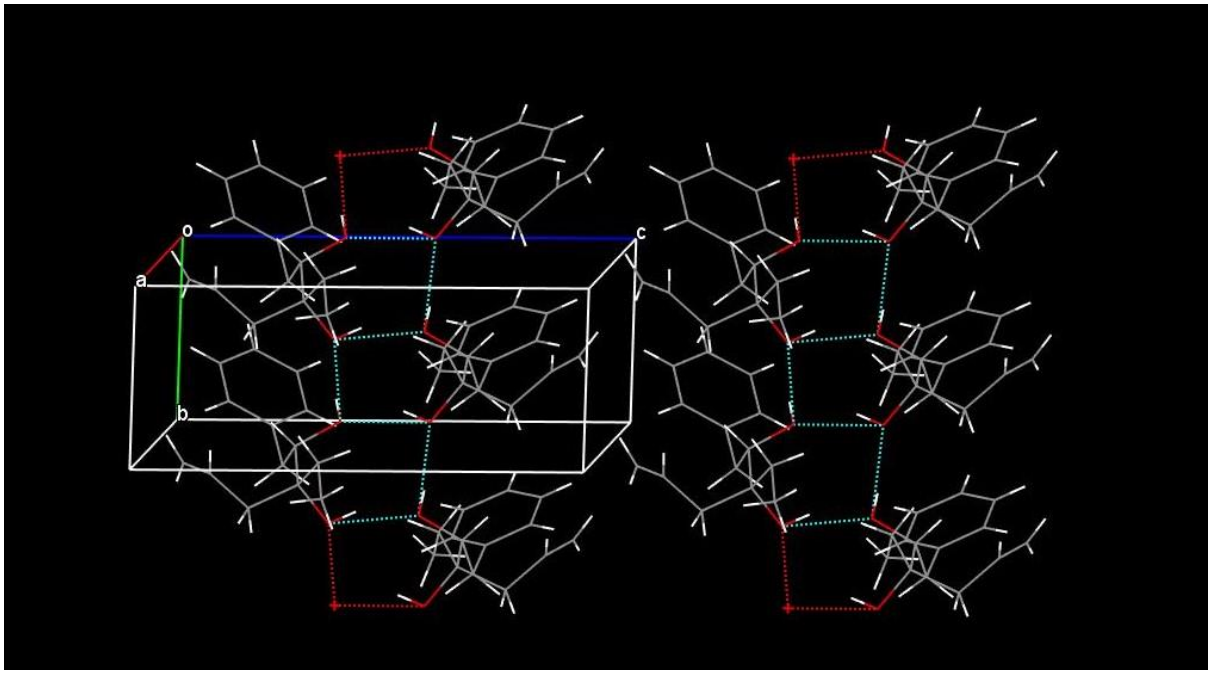

(b)

Figure S1. Hydrogen bonded chain of (2*S*,3*R*)-**ephd** molecules along the unique *b*-axis and *a*-and *c*-axes to the front and right, respectively. (a) the LT structure with $Z' = 2$ shows symmetry-independent chains of hydrogen-bonded molecules with a near doubling of *c*-axis and a slight increase in *a*-axis, compared to the RT structure with $Z' = 1$ (b) in which the adjacent hydrogen-bonded molecular chains are related by a *c*-translation.

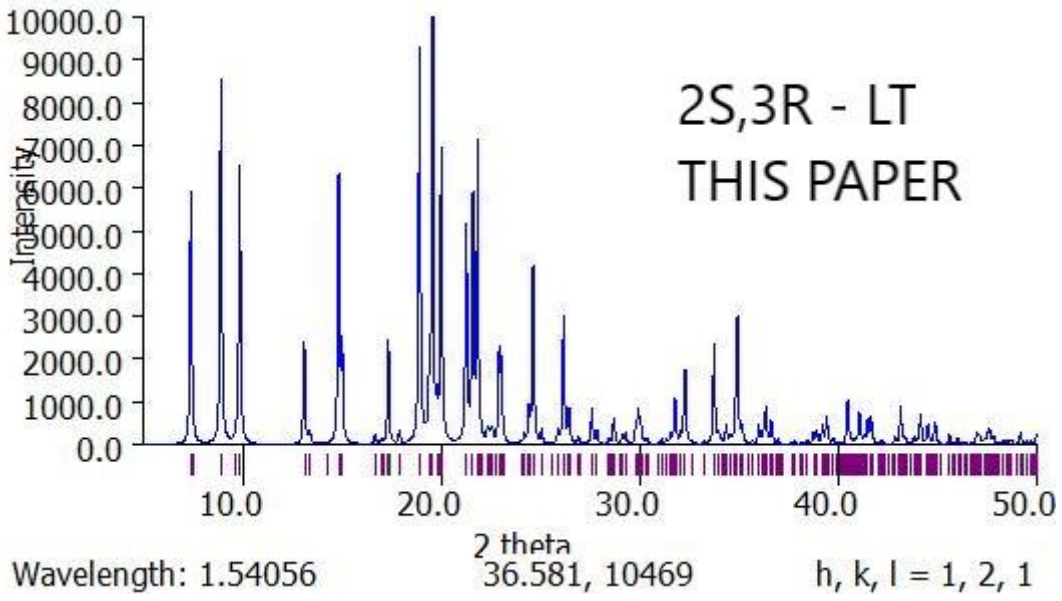

(a)

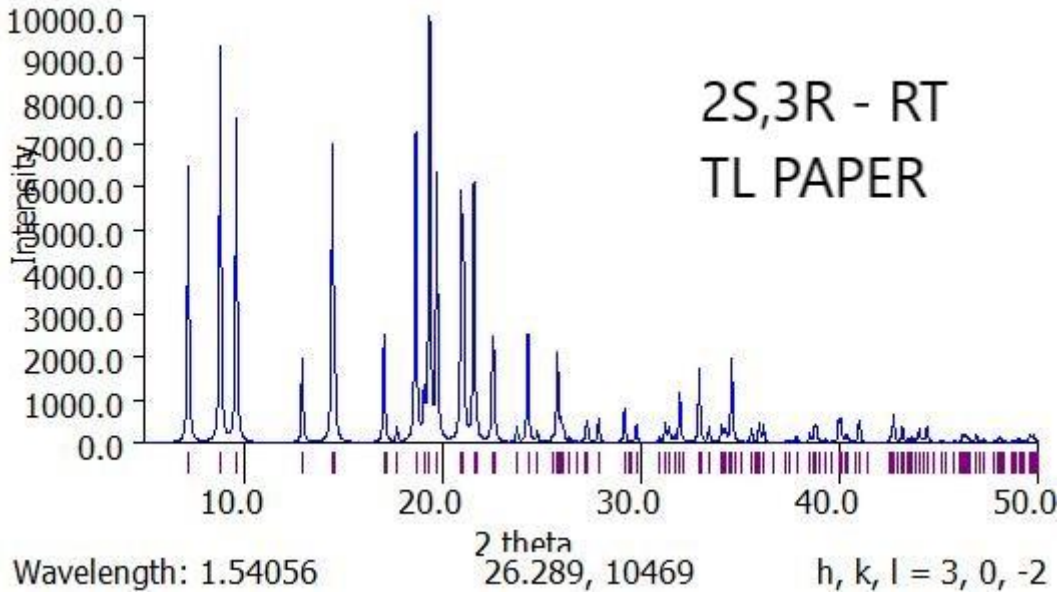
2S,3R - RT
TL PAPER
Intensity
10000.0
9000.0
8000.0
7000.0
6000.0
5000.0
4000.0
3000.0
2000.0
1000.0
0.0
10.0
20.0
30.0
40.0
50.0
2 theta
Wavelength: 1.54056
26.289, 10469
h, k, l = 3, 0, -2

(b)

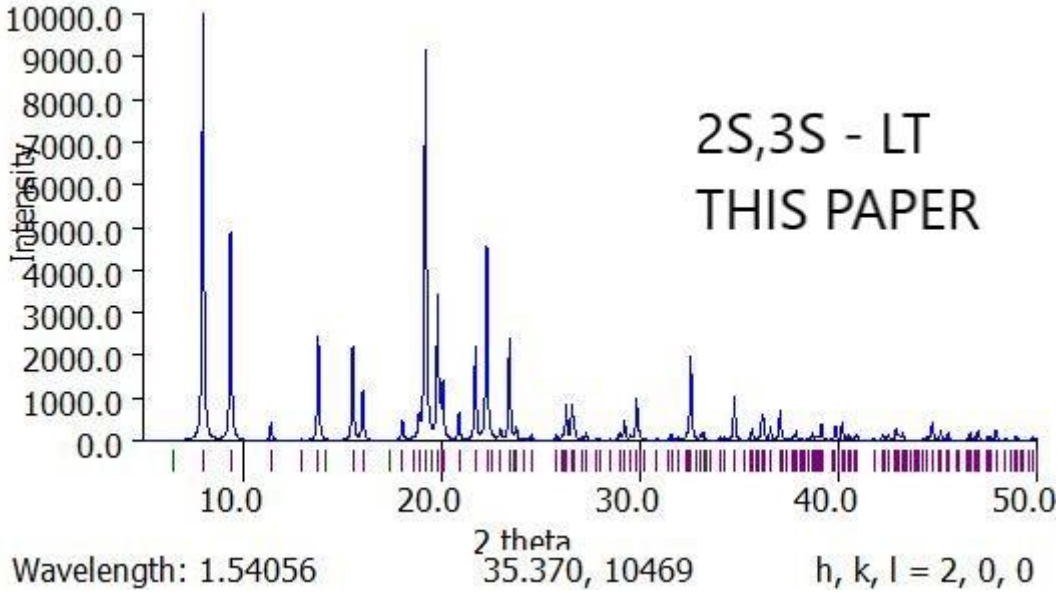
2S,3S - LT
THIS PAPER
Intensity
10000.0
9000.0
8000.0
7000.0
6000.0
5000.0
4000.0
3000.0
2000.0
1000.0
0.0
10.0
20.0
30.0
40.0
50.0
2 theta
Wavelength: 1.54056
35.370, 10469
h, k, l = 2, 0, 0

(c)

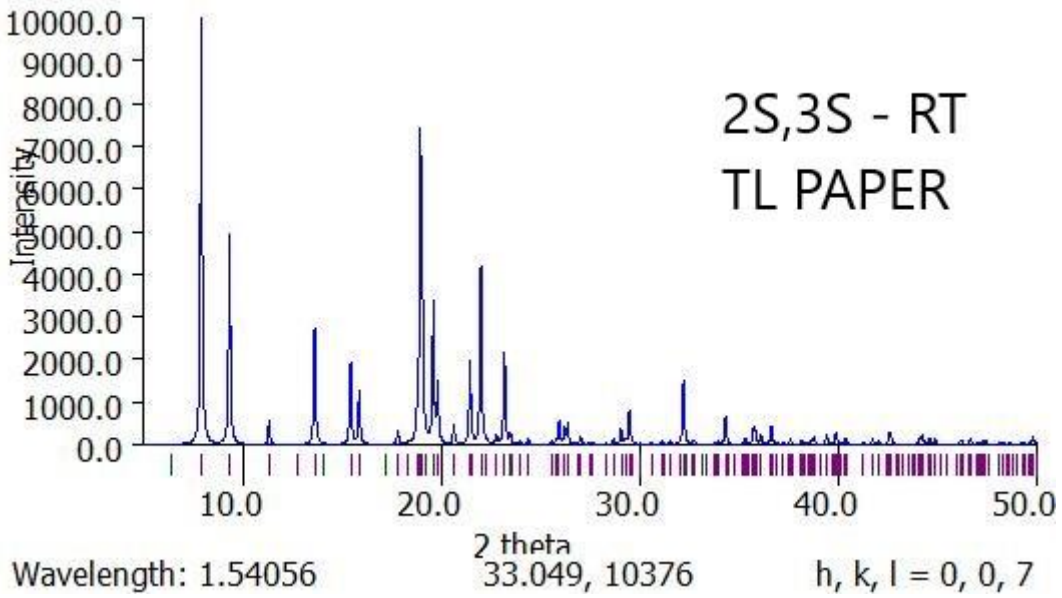

(d)

Figure S2. Calculated PXRD lines of (2*S*,3*R*)-**ephd** at LT (a) and RT (b) are indistinguishable, implying that there are no phase changes in the compound, but the change in Z' with temperature is the frequent modulation of crystal structure. There is no polymorphism or phase change detected by PXRD. The unit cell parameters and PXRD lines of (2*S*,3*S*)-**ephd** at LT (c) and RT (d) are similar, except for nominal T effects.

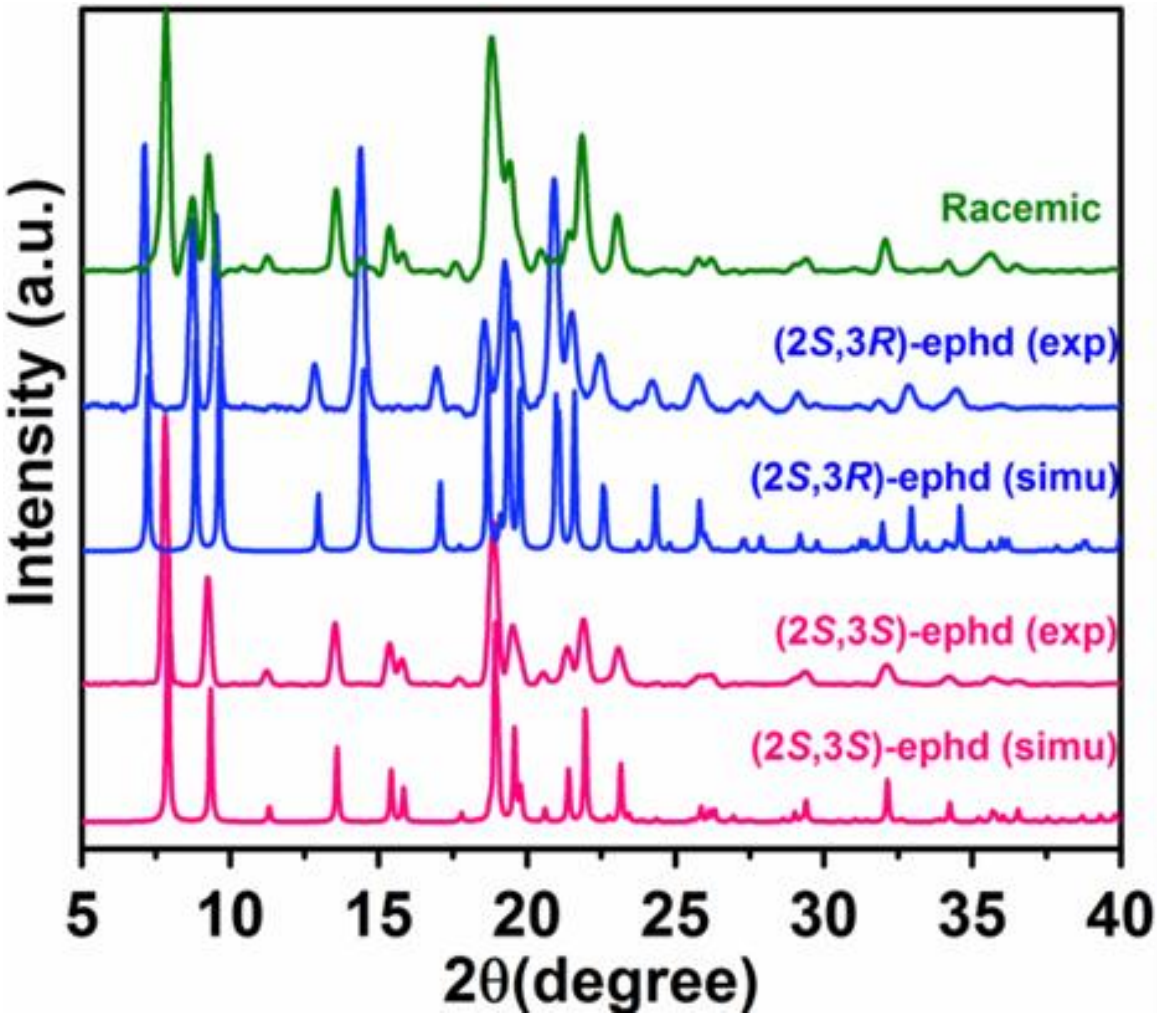

Figure S3. Overlay diagram of experimental and calculated PXRD patterns of (2*S*,3*S*)-**ephd** (magenta) and (2*S*,3*R*)-**ephd** (blue). The mixture of **ephd** diastereomers (racemic) is shown in green color. The PXRD pattern of racemic and individual diastereomeric pairs is distinct, indicating each diastereomer's phase purity (pure). Calculated PXRD line patterns are of the LT single crystal X-ray structures determined in this study. The LT and RT structures PXRDs are almost indistinguishable except fine splitting of a few lines above 20 ° 2θ for (2*S*,3*R*)-**ephd** (see Figures S2).

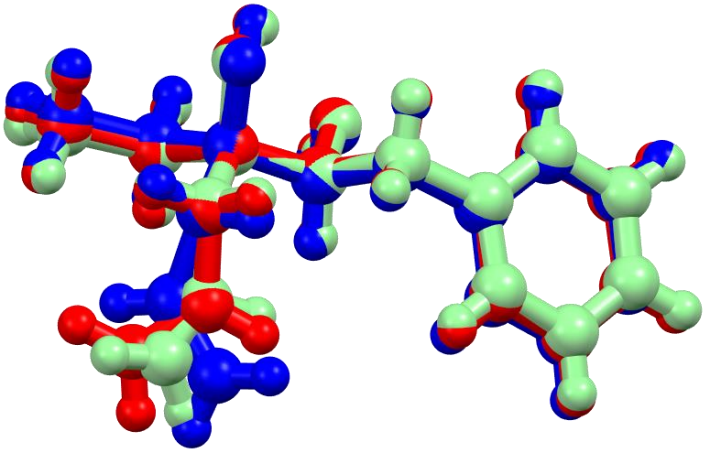

Figure S4. The molecular overlay diagram of (2*S*,3*R*)-**ephd,** in which the molecules shown with Red & Blue color obtained from the 100 K data, while the molecule shown with green color is collected at RT.

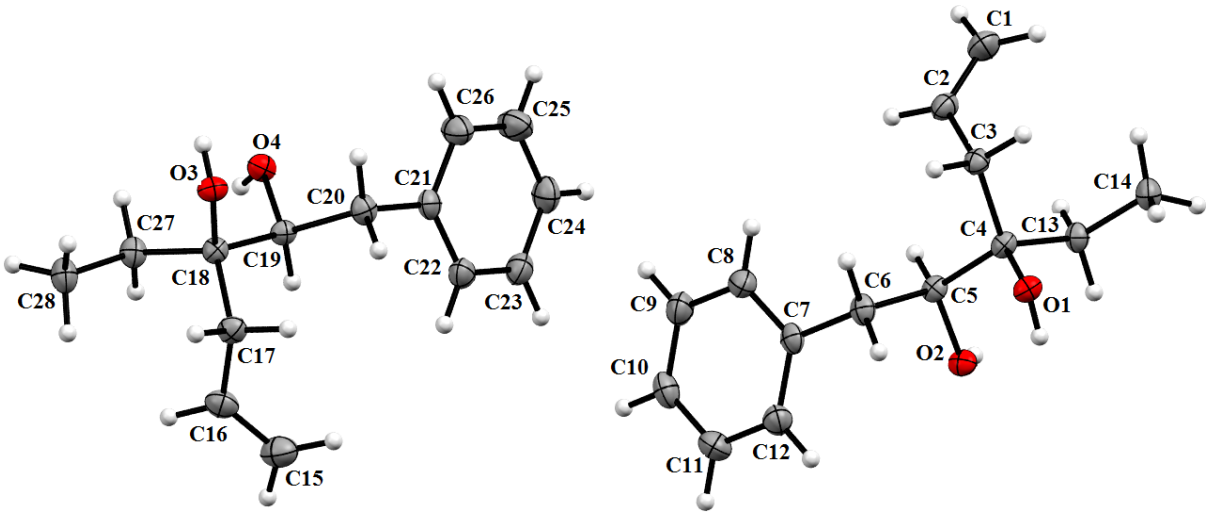

Figure S5. ORTEP diagram of (2*S*,3*R*)–**ephd,** herein, the thermal ellipsoids are drawn with 50% probability. The asymmetric unit contains two molecules.

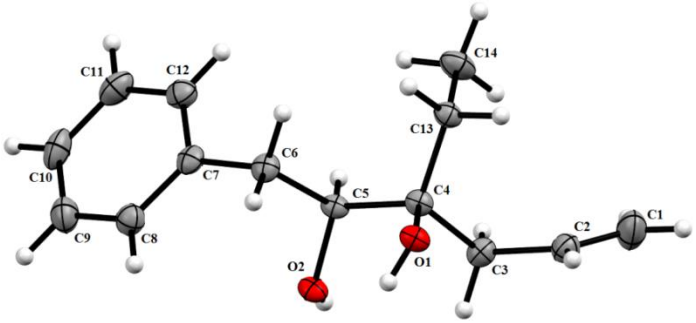

Figure S6. ORTEP diagram of (2*S*,3*S*)–**ephd,** herein, the thermal ellipsoids are drawn with 50% probability. The asymmetric unit contains a single molecule.

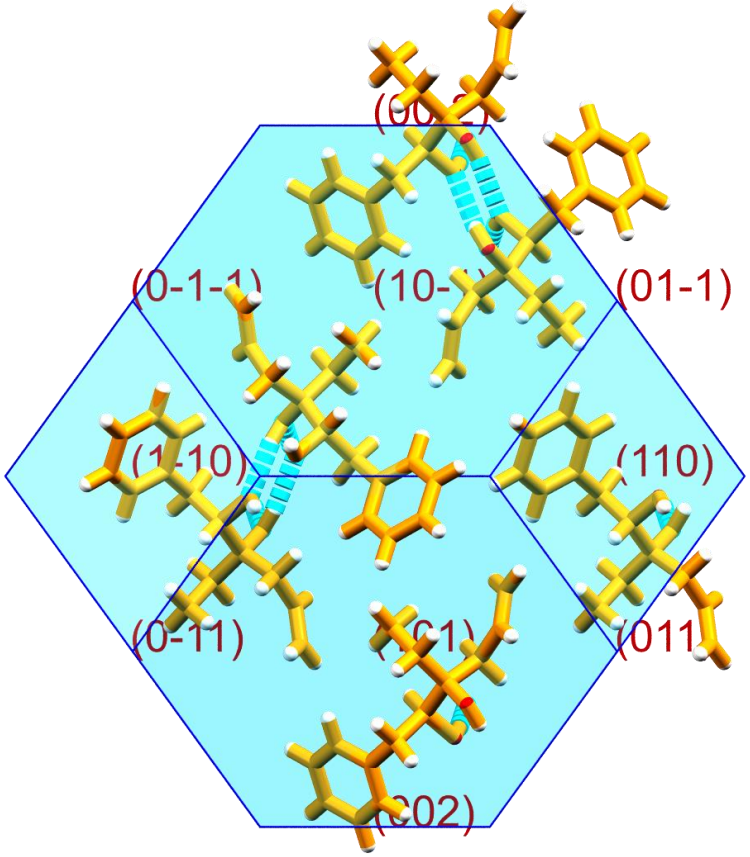

Figure S7. BFDH morphology and the crystal packing arrangement of (2*S*,3*S*)–**ephd** along the *a*-axis.

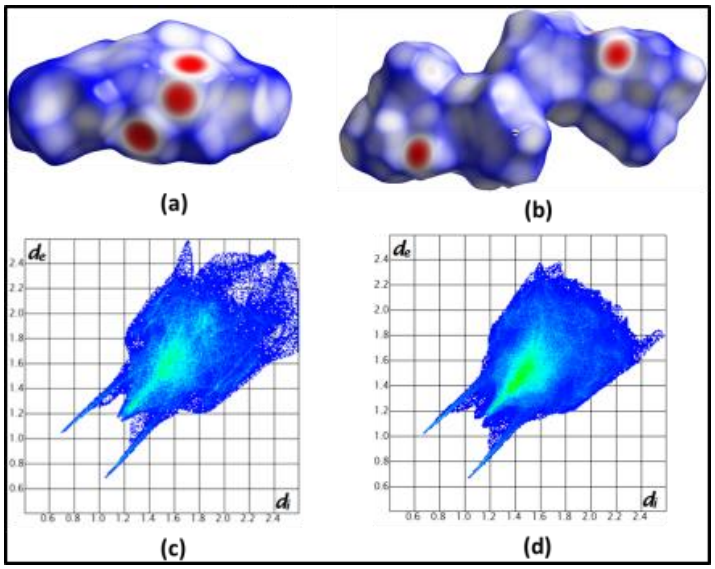

Figure S8. Hirshfeld analysis proposed by Spackman *et al.*,[4] has been applied to both the diastereomers, the Hirshfeld surfaces were generated for (2*S*,3*S*)-**ephd** (a) and (b) for (2*S*,3*R*)-**ephd**.; while the Fingerprint plots generated for (2*S*,3*S*)-**ephd** (c) and (b) for (2*S*,3*R*)-**ephd.**

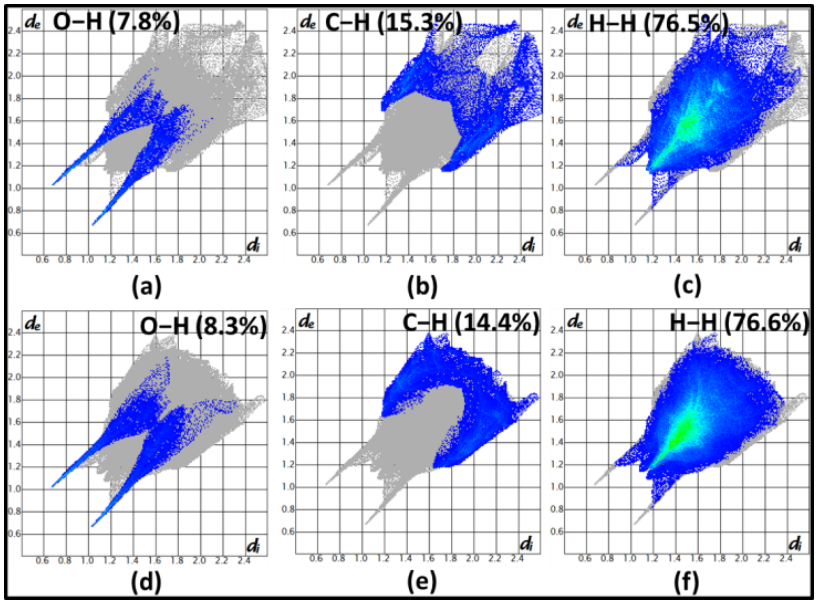

Figure S9. The decomposition of Fingerprints with an appropriate percentage of intermolecular interactions of each type has been given. The interaction percentage of (2*S*,3*S*)-**ephd** is given in (a), (b), and (c); and in (d), (e) and (f) for (2*S*,3*R*)-**ephd**.

References

S1. M. Dandawate, R. Choudhury, G. R. Krishna and D. S. Reddy, *Tetrahedron Lett*, 2020, **61** (47), 152526.

S2. G. M. Sheldrick, SHELXS97 and SHELXL97. Program for Crystal Structure Solution and Refinement. University of Göttingen, Göttingen, 1997.

S3. L. J. Barbour, X-Seed, Graphical Interface to SHELX-97 and POV-Ray; University of Missouri; Columbia: Columbia, MO, 1999.

S4. https://publcif.iucr.org/cifmoldb/mscif/ (accessed 4th August 2021).

S5. M. A. Spackman and D. Jayatilaka, *CrystEngComm*, 2009, **11**, 19.

^{1}H NMR of Compound **1a** in $CDCl_3$ at 400 MHz

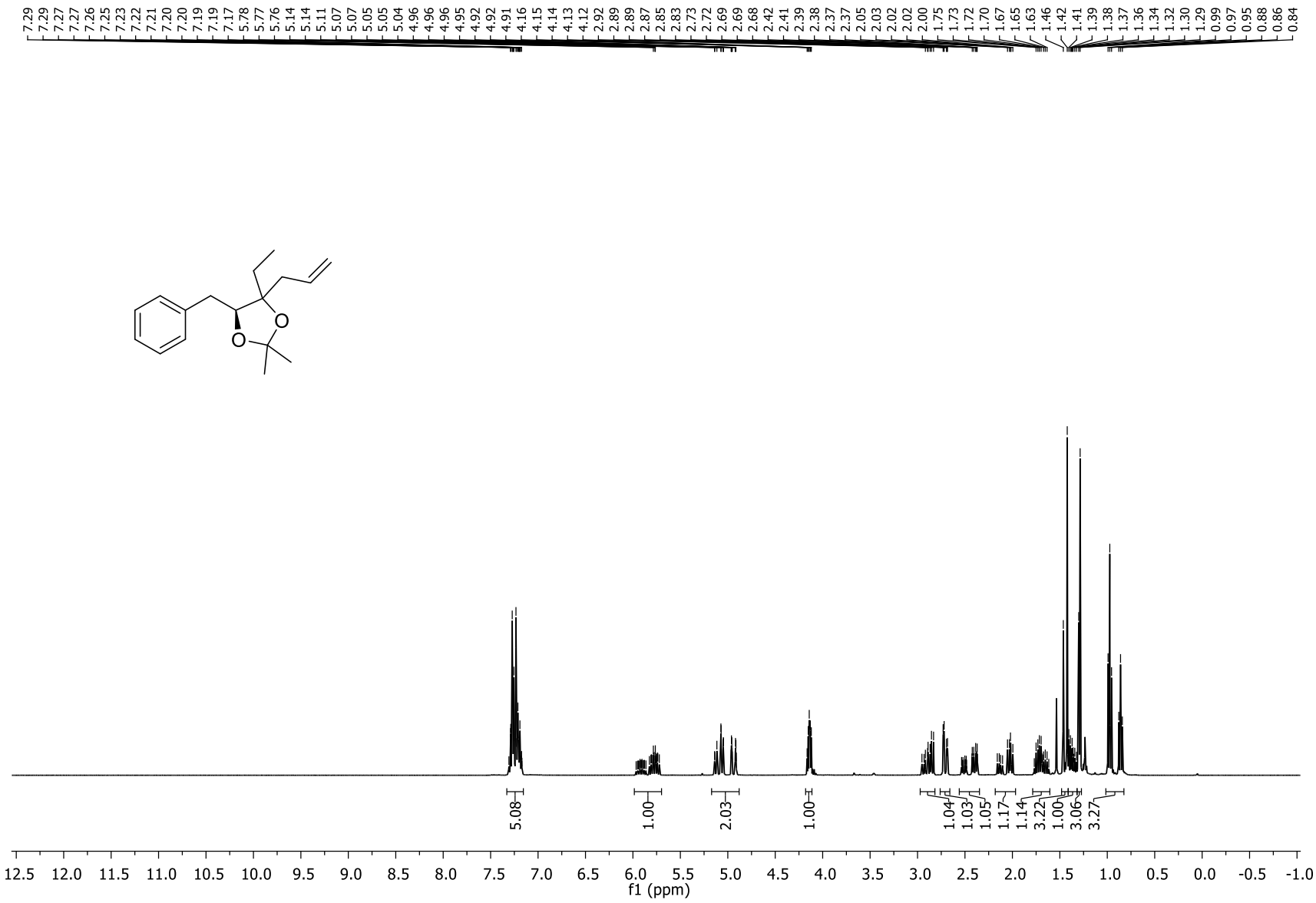

^{13}C NMR of Compound **1a** in $CDCl_3$ at 100 MHz

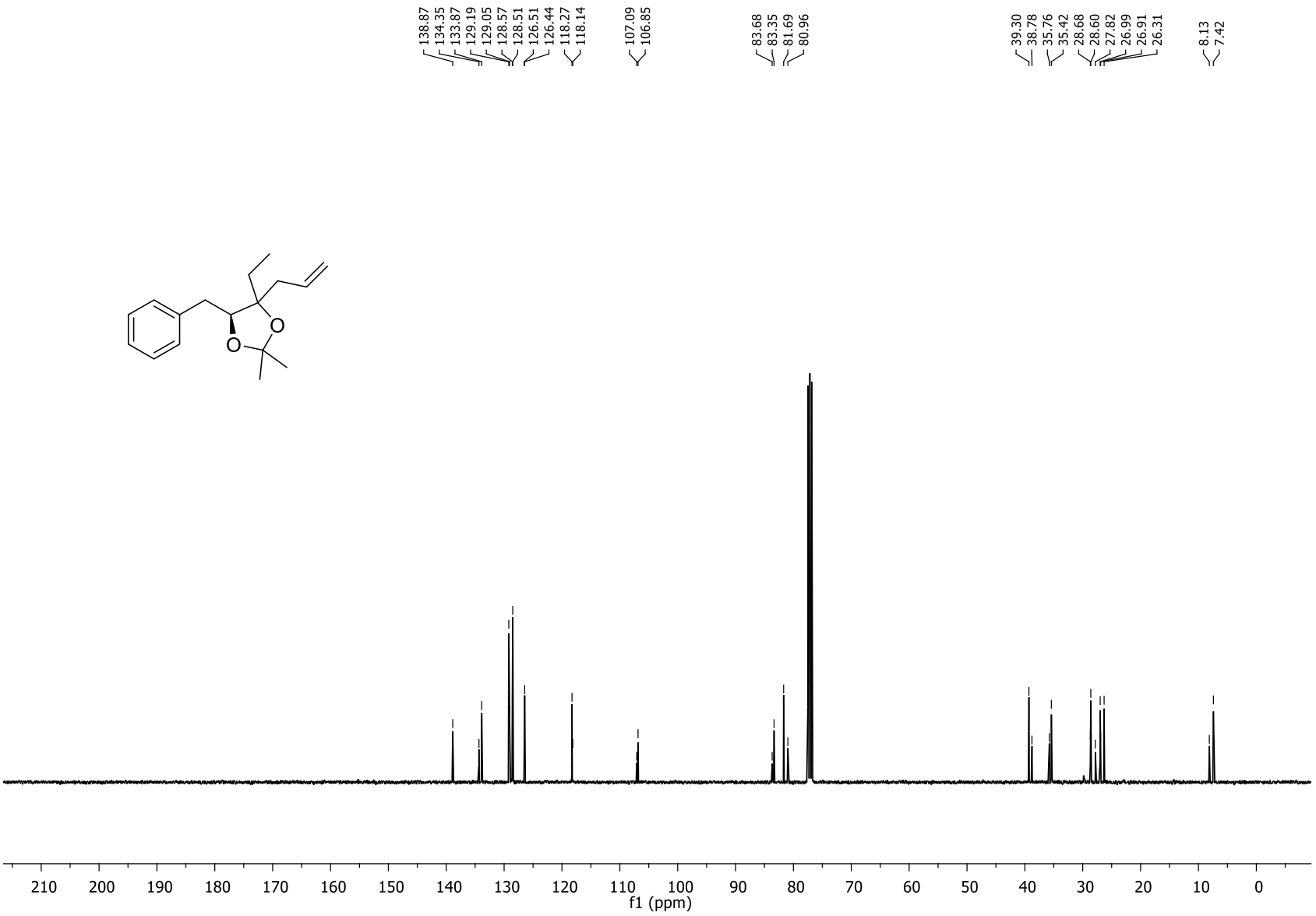

^{1}H NMR of Compound **3a** in $CDCl_3$ at 400 MHz

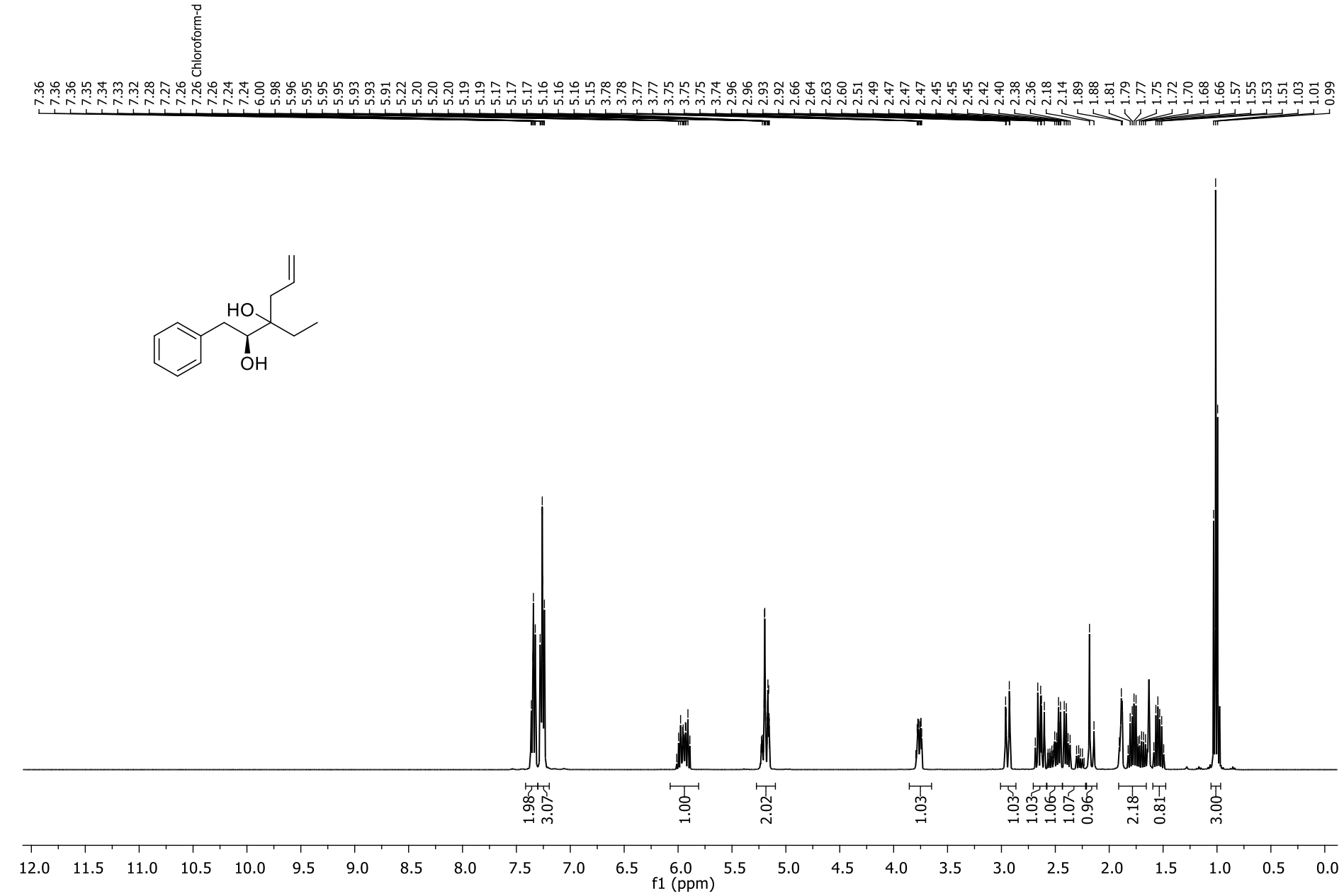

^{13}C NMR of Compound **3a** in $CDCl_3$ at 100 MHz

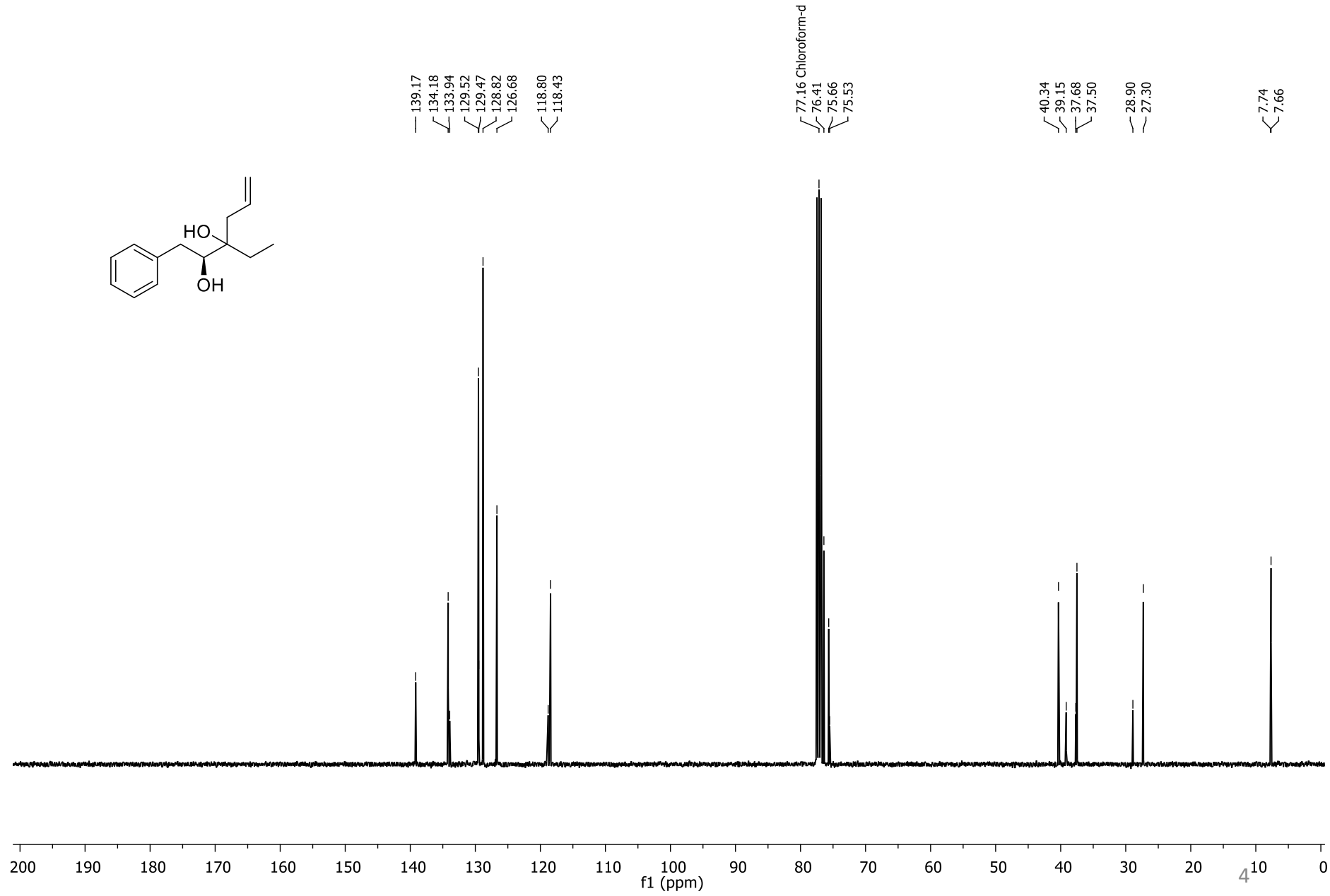

^{1}H NMR of Compound **4a** in $CDCl_3$ at 400 MHz

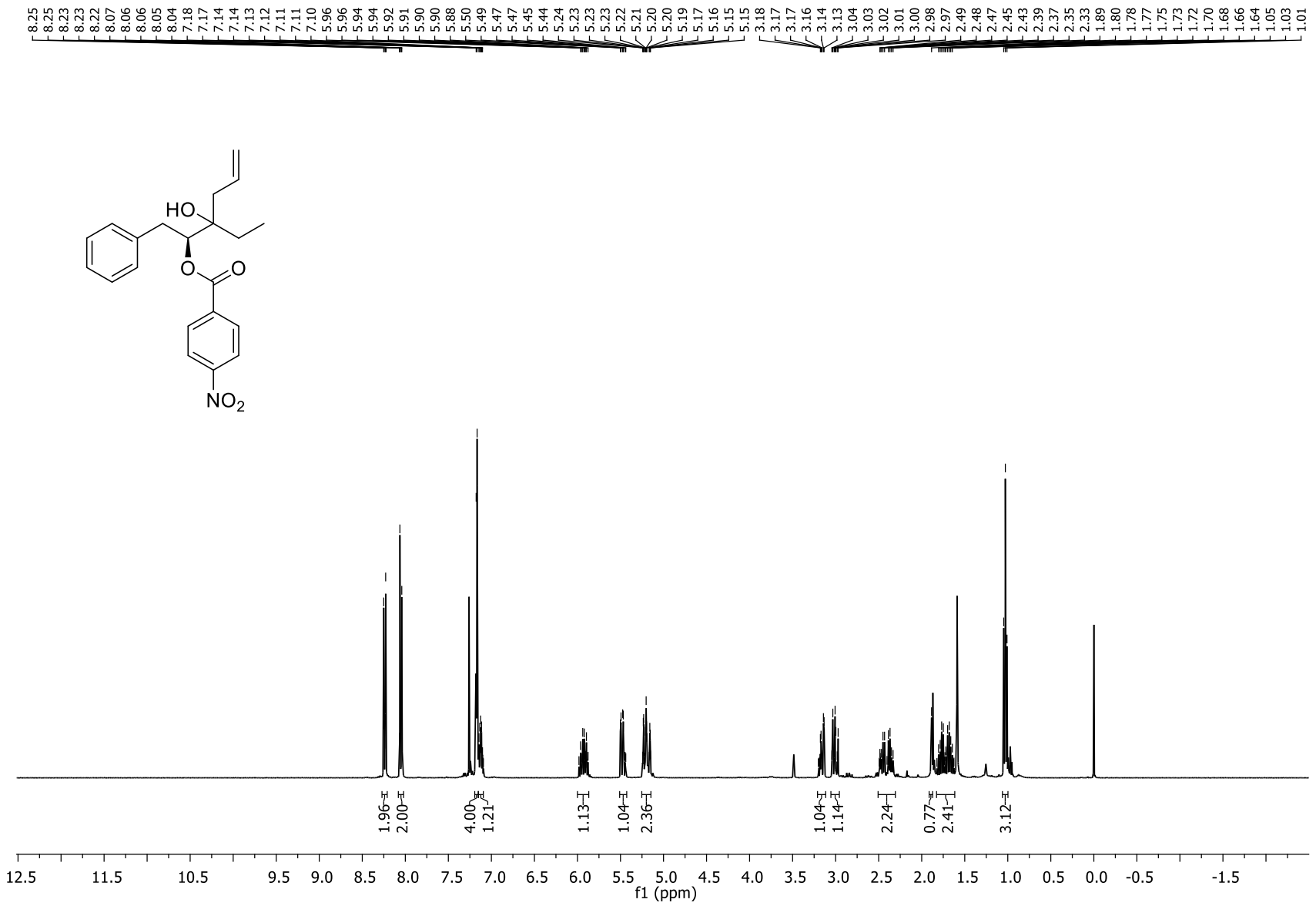

^{13}C NMR of Compound **4a** in $CDCl_3$ at 100 MHz